Editors' Suggestion

Spin excitations of magnetoelectric $LiNiPO_4$ in multiple magnetic phases

L. Peedu,[1] V. Kocsis,[2] D. Szaller,[3] J. Viirok,[1] U. Nagel,[1] T. Rõõm,[1] D. G. Farkas,[4] S. Bordács,[4,5] D. L. Kamenskyi,[6] U. Zeitler,[6] Y. Tokunaga,[2,7] Y. Taguchi,[2] Y. Tokura,[2,8] and I. Kézsmárki[4,9]

[1]*National Institute of Chemical Physics and Biophysics, Akadeemia tee 23, 12618 Tallinn, Estonia*
[2]*RIKEN Center for Emergent Matter Science (CEMS), Wako, Saitama 351-0198, Japan*
[3]*Institute of Solid State Physics, Vienna University of Technology, 1040 Vienna, Austria*
[4]*Department of Physics, Budapest University of Technology and Economics, 1111 Budapest, Hungary*
[5]*Hungarian Academy of Sciences, Premium Postdoctor Program, 1051 Budapest, Hungary*
[6]*High Field Magnet Laboratory (HFML-EMFL), Radboud University, Toernooiveld 7, 6525 ED Nijmegen, The Netherlands*
[7]*Department of Advanced Materials Science, University of Tokyo, Kashiwa 277-8561, Japan*
[8]*Department of Applied Physics, University of Tokyo, Hongo, Tokyo 113-8656, Japan*
[9]*Experimental Physics 5, Center for Electronic Correlations and Magnetism, Institute of Physics, University of Augsburg, 86159 Augsburg, Germany*

(Received 16 April 2019; published 8 July 2019)

Spin excitations of magnetoelectric $LiNiPO_4$ are studied by infrared absorption spectroscopy in the THz spectral range as a function of magnetic field through various commensurate and incommensurate magnetically ordered phases up to 33 T. Six spin resonances and a strong two-magnon continuum are observed in zero magnetic field. Our systematic polarization study reveals that some of the excitations are usual magnetic-dipole active magnon modes, while others are either electromagnons, being only electric-dipole active, or magnetoelectric, that is both electric- and magnetic-dipole active spin excitations. Field-induced shifts of the modes for all three orientations of the field along the orthorhombic axes allow us to refine the values of the relevant exchange couplings, single-ion anisotropies, and the Dzyaloshinskii-Moriya interaction on the level of a four-sublattice mean-field spin model. This model also reproduces the spectral shape of the two-magnon absorption continuum, found to be electric-dipole active in the experiment.

DOI: 10.1103/PhysRevB.100.024406

I. INTRODUCTION

Potential of magnetoelectric (ME) materials in applications relies on the entanglement of magnetic moments and electric polarization [1–8]. Such an entanglement leads not only to the static ME effect but also to the optical ME effect. One manifestation of the optical ME effect is the nonreciprocal directional dichroism, a difference in the absorption with respect to the reversal of light propagation direction [9–12]. The spectrum of nonreciprocal directional dichroism and the linear static ME susceptibility are related via a ME sum rule [13]. According to this sum rule the contribution of simultaneously magnetic- and electric-dipole active spin excitations to the linear ME susceptibility grows as ω^{-2} with $\omega \to 0$. Indeed, strong nonreciprocal directional dichroism has been observed at low frequencies, typically in the GHz-THz range, at spin excitations in several ME materials [14–26]. Besides the interest in the nonreciprocal effect, the knowledge of the spin excitation spectrum and selection rules, i.e., whether the excitations are ordinary magnetic-dipole active magnons, electromagnons (electric-dipole active magnons [27]), or ME spin excitations (simultaneously magnetic- and electric-dipole active spin excitations), is crucial in understanding the origin of static ME effect.

It is well established that the static ME effect is present in several olivine-type $LiMPO_4$ (M = Mn, Fe, Co, Ni) compounds [28–35]. $LiNiPO_4$ is particularly interesting due to many magnetic-field-induced phases, some with incommensurate magnetic order, which is unique in the olivine lithium-orthophosphate family [36]. However, little is known about the spectrum of spin excitations and their selection rules.

THz absorption spectroscopy offers an excellent tool to investigate spin excitation spectra over a broad magnetic field range. As compared to the inelastic neutron scattering (INS), only spin excitations with zero linear momentum are probed, but with a better energy resolution. In addition to excitation frequencies, THz spectroscopy can determine whether the spin excitations are magnetic-dipole active magnons, electromagnons, or ME spin excitations. This information is essential for developing a spin model that would describe the ground and the low-lying excited states of the material.

We studied the spin excitation spectra of $LiNiPO_4$ in magnetic field using THz absorption spectroscopy. In the previous INS works two magnon branches were observed below 8 meV [36–38]. Here we broaden the spectral range up to 24 meV, which allows us to observe additional spin excitations and to identify the polarization selection rules for the spin excitations. Using a mean-field model we describe the field dependence of the magnetization and the magnon energies in commensurate phases, from where we refine the values of exchange couplings, single-ion anisotropies, and the Dzyaloshinskii-Moriya interaction. Besides magnons described by the mean-field model, few other spin excitations, including two-magnon excitations, are observed.

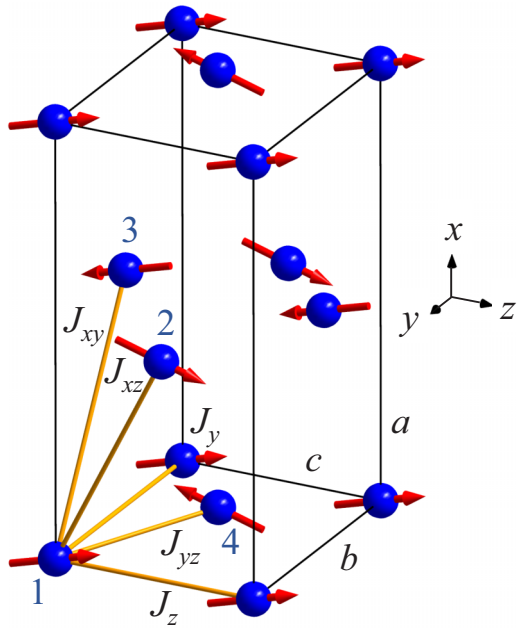

FIG. 1. The ground-state spin configuration of $LiNiPO_4$ in zero magnetic field. There are four Ni^{2+} spins, $S = 1$, in the magnetic unit cell drawn as a box. The spins are canted away from the z axis towards the x axis by $\theta = \pm(7.8^\circ \pm 2.6^\circ)$ [36,39]. The numbering of spins and the labeling of exchange interactions corresponds to the spin Hamiltonian described by Eq. (1).

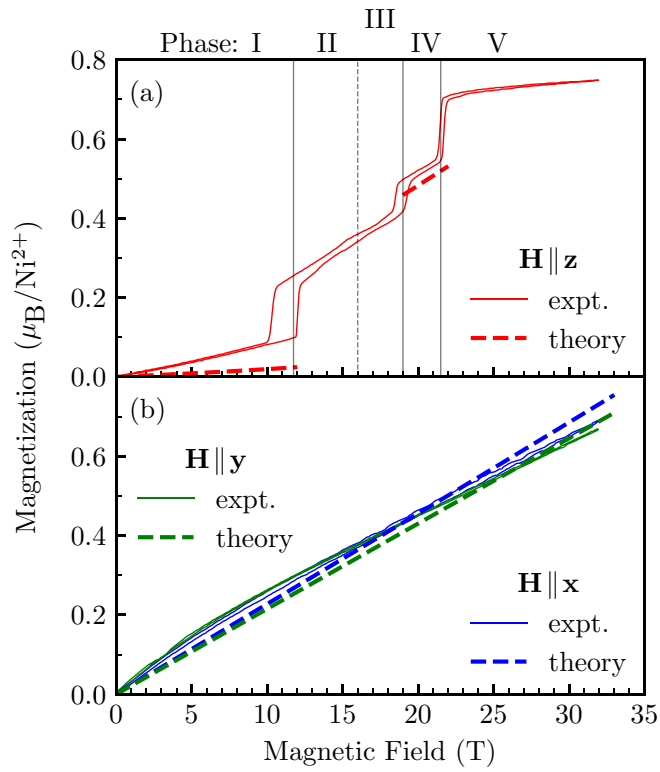

FIG. 2. Magnetic field **H** dependence of the magnetization **M** parallel to the field at 2.4 K. (a) **H** ∥ **z**, (b) **H** ∥ **y** (green) and **H** ∥ **x** (blue). Solid lines are experimental results and the dashed lines are calculated from the mean-field model with the parameters of this work listed in Table I.

$LiNiPO_4$ has orthorhombic symmetry with space group *Pnma*. The magnetic Ni^{2+} ion with spin $S = 1$ is inside a distorted O_6 octahedron. There are four Ni^{2+} ions in the structural unit cell forming buckled planes perpendicular to the crystal x axis, as shown in Fig. 1. The nearest-neighbor spins in the yz plane are coupled by strong AF exchange interaction which results in a commensurate AF order below $T_N = 20.8$ K [40,41]. The ordered magnetic moments are almost parallel to the crystallographic z axis with slight canting towards the x direction [42]. On heating above T_N the material undergoes a first-order phase transition into a long-range incommensurate magnetic structure. Further heating results in a second-order phase transition into the paramagnetic state at $T_{IC} = 21.7$ K, while short-range magnetic correlations persist up to 40 K [41]. Owing to the competing magnetic interactions $LiNiPO_4$ has a very rich H-T phase diagram with transitions appearing as multiple steps in the field dependence of the magnetization [43,44]. The delicate balance of the nearest-neighbor and the frustrated next-nearest-neighbor exchange interactions puts the material on the verge of commensurate and incommensurate structures, which alternate in increasing the magnetic field applied along the z axis as shown in Fig. 2(a) [37,38,42].

II. EXPERIMENTAL DETAILS

$LiNiPO_4$ single crystals were grown by the floating zone method, similarly as described in Ref. [45]. Crystal quality was tested by 2-θ and Laue x-ray diffraction, which reconfirmed the orthorhombic structure with the same lattice constants as reported in Ref. [46]. Three samples each with a large face normal to one of the principal axes were cut from the same ingot. For optical measurements the slabs with thicknesses from 0.87 to 1.09 mm had an approximately 2° wedge to suppress interference caused by internal reflections. Samples were mounted on metal discs where the hole depending on the sample size limited the THz beam cross section to 8–16 mm^2.

THz measurements up to 17 T were performed in Tallinn with a Martin-Puplett interferometer and a 0.3-K silicon bolometer. High-field spectra from 17 T up to 33 T were measured in the Nijmegen High Field Magnet Laboratory using a Bruker IFS 113v spectrometer and a 1.6-K silicon bolometer. The experiments above 17 T were done in the Faraday configuration (**k** ∥ **H**), while below 17 T both the Faraday and the Voigt (**k** ⊥ **H**) configuration experiments were performed. All spectra were measured with an apodized spectral resolution of 0.5 cm^{-1}. A linear polarizer was mounted in front of the sample to control the polarization state of the incoming light.

Absorption was determined by using a reference spectrum. The reference spectrum was obtained on the sample in zero magnetic field in the paramagnetic state at $T = 30$ K or by measuring a reference hole with the area equal to the sample hole area. In the former case the relative absorption is calculated as $\alpha(H,T) - \alpha(0\,\mathrm{T}, 30\,\mathrm{K}) = -d^{-1} \ln[I(H,T)/I(0\,\mathrm{T}, 30\,\mathrm{K})]$ where d is the sample thickness and I is the measured intensity. In the latter case the

absolute absorption is calculated as $\alpha = -d^{-1}\ln(I/I_r)$ where I_r is the intensity through the reference hole.

Magnetization up to 32 T was measured in the Nijmegen High Field Magnet Laboratory on a Bitter magnet with a vibrating-sample magnetometer (VSM) and additional low-field measurements were done using a 14-T PPMS with VSM option (Quantum Design).

III. MEAN-FIELD MODEL AND MAGNONS

The terms included in the spin Hamiltonian, exchange interactions, single-ion anisotropy terms, and the Zeeman energy correspond to those also considered in earlier works on $LiNiPO_4$ [36–38]. The model contains four spin variables as classical vectors $\{\mathbf{S}_1, \mathbf{S}_2, \mathbf{S}_3, \mathbf{S}_4\}$ in accordance with the four crystallographically nonequivalent positions of the spin $S = 1$ Ni^{2+} ions in $LiNiPO_4$. The four spins of the magnetic unit cell are connected by five different exchange couplings as presented in Fig. 1. Two of these couplings, J_y and J_z, connect spins at the same crystallographic sites producing, irrespective of the spin state, a constant energy shift in the Γ point within the four-sublattice model. Although these terms are omitted in the analysis of single-magnon excitations, they become relevant in the analysis of two-magnon excitations as discussed in Sec. B. The spin Hamiltonian of the magnetic unit cell in the four-sublattice model reads

$$\begin{aligned}\mathcal{H} = \sum_{i=1}^{4} &\left[\Lambda_x\left(S_i^x\right)^2 + \Lambda_y\left(S_i^y\right)^2 - g\mu_B\mu_0\mathbf{H}\cdot\mathbf{S}_i\right] \\ &+ 4\big[J_{xz}(\mathbf{S}_1\cdot\mathbf{S}_2 + \mathbf{S}_3\cdot\mathbf{S}_4) + J_{xy}(\mathbf{S}_1\cdot\mathbf{S}_3 + \mathbf{S}_2\cdot\mathbf{S}_4) \\ &+ J_{yz}(\mathbf{S}_1\cdot\mathbf{S}_4 + \mathbf{S}_2\cdot\mathbf{S}_3) \\ &+ D_y\left(S_1^zS_4^x - S_1^xS_4^z + S_3^zS_2^x - S_3^xS_2^z\right)\big]. \end{aligned} \tag{1}$$

Due to the strongly distorted ligand cage of the magnetic ion, the orthorhombic anisotropy of the crystal is taken into account by two single-ion hard-axis anisotropies, $\Lambda_x, \Lambda_y > 0$. The parameters in the Zeeman term are the g factor g, the Bohr magneton μ_B, and the vacuum permeability μ_0. Parameters J_{xz}, J_{xy}, and J_{yz} are the isotropic Heisenberg exchange couplings as shown in Fig. 1, while D_y is the Dzyaloshinskii-Moriya interaction.

According to the neutron-diffraction studies [47,48] the ground-state spin configuration of $LiNiPO_4$ in zero magnetic field is a predominantly collinear AF order, where $\mathbf{S}_1$ and $\mathbf{S}_2$ point in $+z$, while $\mathbf{S}_3$ and $\mathbf{S}_4$ in the $-z$ direction, shown in Fig. 1. Thus, the dominant exchange interaction is the AF $J_{yz} > 0$ coupling, while z is an easy axis as $\Lambda_x, \Lambda_y > 0$. On top of the collinear order a small alternating canting of spins with net spin along x is superimposed [39]. Canting is induced by the Dzyaloshinskii-Moriya coupling D_y and breaks the equivalence of $\mathbf{S}_1$ and $\mathbf{S}_2$ as well as $\mathbf{S}_3$ and $\mathbf{S}_4$. The canting angle θ measured from the z axis is approximately

$$\tan\theta \approx \frac{2D_y}{\Lambda_x - 4(J_{xz} - J_{yz})}. \tag{2}$$

At each magnetic field, the ground-state spin configuration is obtained by minimizing the energy corresponding to Eq. (1).

The resonance frequencies and amplitudes of modes are calculated using the Landau-Lifshitz equation [49]

$$\dot{\mathbf{S}}_i = -\frac{1}{\hbar}\mathbf{S}_i \times \frac{\partial\,\mathcal{H}}{\partial\,\mathbf{S}_i}, \tag{3}$$

where $\dot{\mathbf{S}}_i \equiv d\mathbf{S}_i/dt$.

We solve Eq. (3) for small spin deviations $\{\delta\mathbf{S}\} \equiv \{\delta\mathbf{S}_1, \ldots \delta\mathbf{S}_N\}$ from the equilibrium $\{\mathbf{S}^0\} \equiv \{\mathbf{S}_1^0, \ldots \mathbf{S}_N^0\}$, where $\{\mathbf{S}\} = \{\mathbf{S}^0\} + \{\delta\mathbf{S}\}$, with N spins in the magnetic unit cell. It follows from Eq. (3) that $\delta\mathbf{S}_i \perp \mathbf{S}_i$, leaving the spin length constant in the first order of $\delta\mathbf{S}_i$. Inserting $\{\mathbf{S}\}$ into Landau-Lifshitz Eq. (3) and keeping only terms linear in $\delta\mathbf{S}_i$ (terms zero order in $\delta\mathbf{S}_i$ add up to zero) we get

$$\delta\dot{\mathbf{S}}_i = -\frac{1}{\hbar}\mathbf{S}_i^0 \times \frac{\partial\,\mathcal{H}_\delta}{\partial\,\mathbf{S}_i}, \tag{4}$$

where the effective field is

$$\frac{\partial\,\mathcal{H}_\delta}{\partial\,\mathbf{S}_i} = \left.\frac{\partial\,\mathcal{H}}{\partial\,\mathbf{S}_i}\right|_{\{\mathbf{S}^0\}+\{\delta\mathbf{S}\}}. \tag{5}$$

We solve Eq. (4) by assuming harmonic time dependence $\delta\mathbf{S}_i(t) = \delta\mathbf{S}_i\exp(i\omega t)$. The number of modes is equal to the number of spins in the unit cell.

To calculate the absorption of electromagnetic waves by the magnons we introduce damping. The Landau-Lifshitz-Gilbert equation [50] for the ith spin is

$$\dot{\mathbf{S}}_i = -\frac{1}{\hbar}\mathbf{S}_i \times \frac{\partial\,\mathcal{H}_\delta}{\partial\,\mathbf{S}_i} + \frac{\alpha}{\hbar S_i}\mathbf{S}_i \times \mathbf{S}_i \times \frac{\partial\,\mathcal{H}_\delta}{\partial\,\mathbf{S}_i}, \tag{6}$$

where α is a positive dimensionless damping parameter and small, $\alpha \ll 1$. Using $\mathbf{A}\times\mathbf{B}\times\mathbf{C} = \mathbf{B}(\mathbf{A}\cdot\mathbf{C}) - \mathbf{C}(\mathbf{A}\cdot\mathbf{B})$, and adding a weak harmonic alternating magnetic field, $\mathbf{H}^\omega(t) = \mathbf{H}^\omega\exp(i\omega t)$, to the effective field yields the following form of the equation of motion up to terms linear in $\delta\mathbf{S}_i$ and $\mathbf{H}^\omega$:

$$\begin{aligned}\delta\dot{\mathbf{S}}_i = &-\frac{1}{\hbar}\mathbf{S}_i^0 \times \left[\frac{\partial\,\mathcal{H}_\delta}{\partial\,\mathbf{S}_i} - \mu_0\mathbf{H}^\omega(t)\right] \\ &+ \frac{\alpha}{\hbar}\frac{\mathbf{S}_i^0}{S_i^0}\mathbf{S}_i^0 \cdot \left[\frac{\partial\,\mathcal{H}_\delta}{\partial\,\mathbf{S}_i} - \mu_0\mathbf{H}^\omega(t)\right] \\ &- \frac{\alpha}{\hbar}S_i^0\left[\frac{\partial\,\mathcal{H}_\delta}{\partial\,\mathbf{S}_i} - \mu_0\mathbf{H}^\omega(t)\right]. \end{aligned} \tag{7}$$

The absorption of electromagnetic waves by the spin system related to magnetic dipole excitations is calculated from Eq. (7) by inserting $\delta\mathbf{S}_i(t) = \delta\mathbf{S}_i\exp(i\omega t)$ and $\mathbf{H}^\omega(t) = \mathbf{H}^\omega\exp(i\omega t)$. The frequency-dependent magnetic susceptibility tensor $\hat{\chi}(\omega)$ is obtained by summing up all the magnetic moments in the unit cell, $\mathbf{M} = \gamma\hbar\sum_{i=1}^{N}\mathbf{S}_i$ in Eq. (7), and making a transformation into form

$$\gamma\hbar\left[\sum_{i=1}^{M}\delta\mathbf{S}_i(t)\right] = \hat{\chi}(\omega)\mu_0\mathbf{H}^\omega(t). \tag{8}$$

The absorption coefficient is $\alpha_{i,j} = 2\omega c_0^{-1}\mathrm{Im}\,\mathcal{N}_{i,j}$, where the complex index of refraction is $\mathcal{N}_{i,j} = \sqrt{\epsilon_{ii}\mu_{jj}}$ assuming small polarization rotation and negligible linear magnetoelectric susceptibilities χ_{ij}^{em}, χ_{ji}^{me}. The magnetic permeability is $\mu_{jj}(\omega) = 1 + \chi_{jj}(\omega)$ and the background dielectric permittivity is ϵ_{ii}. The polarization of incident radiation is defined as

TABLE I. The parameters of the mean-field model used to describe the static magnetic properties and single- and two-magnon excitations in $LiNiPO_4$: exchange couplings J_{ij} and J_k, single-ion anisotropy constants Λ_i, Dzyaloshinskii-Moriya coupling D_y, and g factor g. Units are in meV except the dimensionless g.

J_y	J_z	J_{xz}	J_{xy}	J_{yz}	Λ_x	Λ_y	D_y	g	Ref.
0.65	0.16	−0.17	0.16	1.24	0.14	0.74	0.41	2.2	[a]
0.67	−0.06	−0.11	0.32	1	0.41	1.42	0.32	2.2	[36]
0.67	−0.05	−0.11	0.3	1.04	0.34	1.82			[37]
0.59	−0.11	−0.16	0.26	0.94	0.34	1.92			[38]

[a]This work.

$\{E_i^\omega, H_j^\omega\}$ where i and j are x, y, or z. If $\chi_{jj}(\omega) \ll 1$,

$$\mathcal{N}_{i,j} \approx \sqrt{\epsilon_{ii}}\left[1 + \frac{\chi_{jj}(\omega)}{2}\right]. \tag{9}$$

Thus, for real ϵ_{ii} the absorption is

$$\alpha_{i,j}(\tilde{\omega}) = 2\pi\tilde{\omega}\sqrt{\epsilon_{ii}}\,\mathrm{Im}\,\chi_{jj}(\tilde{\omega}), \tag{10}$$

where units of wave number are used, $[\tilde{\omega}_n] = \mathrm{cm}^{-1}$.

The values of magnetic interactions and anisotropies obtained in this work, see Table I, reproduce the magnetic field dependence of the magnetization, canting angle θ, and frequencies of four single-spin excitations and a two-magnon excitation in the I and a single-spin excitation in the IV commensurate magnetic phase of $LiNiPO_4$.

IV. EXPERIMENTAL RESULTS

The $LiNiPO_4$ samples were characterized by measuring the magnetization along the x, y, and z directions, shown in Fig. 2. The magnetization increases continuously for $\mathbf{H} \parallel \mathbf{x}$ and $\mathbf{H} \parallel \mathbf{y}$, while for $\mathbf{H} \parallel \mathbf{z}$ there is step at 12, 19, and 21.5 T. These steps correspond to magnetic-field-induced changes in the ground-state spin structure. Phases I and IV are commensurate, while II, III, and V are incommensurate [36,44]. The boundary between phases II and III at 16 T, where the periodicity of the incommensurate spin structure changes [36], is hardly visible in the magnetization data [42,44]. The size of the magnetic unit cells is the same in phases I and IV [44], i.e., four spins as shown in Fig. 1.

The zero-field THz absorption spectra measured at 3.5 K are shown in Fig. 3. Three absorption lines are identified as magnetic-dipole active magnons: $\nu_1 = 16.1\ \mathrm{cm}^{-1}$, $\nu_2 = 36.2\ \mathrm{cm}^{-1}$, and $\nu_3 = 48.4\ \mathrm{cm}^{-1}$. The excitation $\nu_5 = 56.4\ \mathrm{cm}^{-1}$ is an E_y^ω-active electromagnon. The excitations $\nu_4 = 54.8\ \mathrm{cm}^{-1}$ and $\nu_6 = 66.4\ \mathrm{cm}^{-1}$ are ME spin excitations; ν_4 is $\{E_x^\omega, H_z^\omega\}$ active, while ν_6 is present in five different combinations of oscillating electric and magnetic fields with the strongest intensity in E_z^ω polarization; see Table II. There is an E_x^ω-active broad absorption band ν_7.

All seven modes $\nu_1, \ldots, \nu_7$ are absent above T_N. Since no sign of structural changes has been found in the neutron diffraction [39] and in the spectra of Raman-active phonons at T_N [51], the lattice vibrations can be excluded and all new modes are assigned to spin excitations of $LiNiPO_4$.

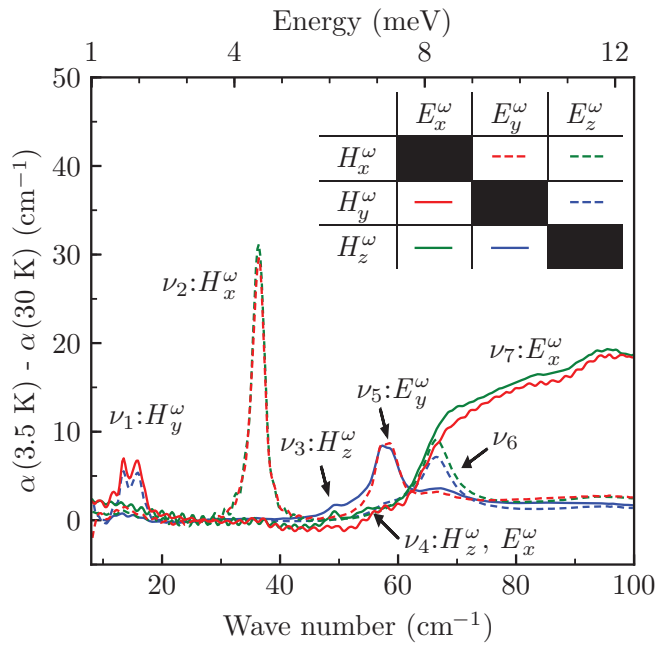

FIG. 3. THz absorption spectra of spin excitations in $LiNiPO_4$ in $H = 0$ at $T = 3.5$ K. Directions of THz radiation propagation are $\mathbf{k} \parallel \mathbf{x}$ (blue), $\mathbf{k} \parallel \mathbf{y}$ (green), and $\mathbf{k} \parallel \mathbf{z}$ (red). Two orthogonal THz radiation polarizations for a given $\mathbf{k}$ vector direction are indicated by solid and dashed lines. Directions of the oscillating THz fields $\{E_i^\omega, H_j^\omega\}$ are indicated in the inset. ν_n labels the modes, $n = 1, \ldots, 7$, with H_j^ω or E_i^ω indicating the magnetic- or electric-dipole activity of the mode, respectively. ν_4 and ν_6 are ME excitations (for the characterization of ν_6 see Table II).

The magnetic field dependence of resonance frequencies and absorption line areas is presented in Fig. 4 as obtained from the fits of the absorption peaks with the Gaussian line shapes. When the magnetic field is applied in $\mathbf{H} \parallel \mathbf{x}$ or $\mathbf{H} \parallel \mathbf{y}$ directions, Fig. 4(a) or 4(b), we found a continuous evolution of modes up to the highest field of 33 T. On the contrary, for $\mathbf{H} \parallel \mathbf{z}$ we observed discontinuities in the spin excitation frequencies, approximately at 12, 19, and 21.5 T. These fields correspond to the field values where the steps are seen in the magnetization in Fig. 2. The boundary between II and III at 16 T is not visible in the THz spectra. Apparently the spin excitation spectra are rather insensitive to the change of the magnetic unit-cell size within the incommensurate phase.

The mean-field model (Sec. III) predicts four magnon modes for a four sublattice system and they are assigned to

TABLE II. The excitation configurations of ME mode ν_6. The area of the symbol is approximately proportional to the absorption line area. The color coding is the same as in Fig. 3.

ν_6	E_x^ω	E_y^ω	E_z^ω
H_x^ω		○	◌
H_y^ω			◌
H_z^ω	○	○	

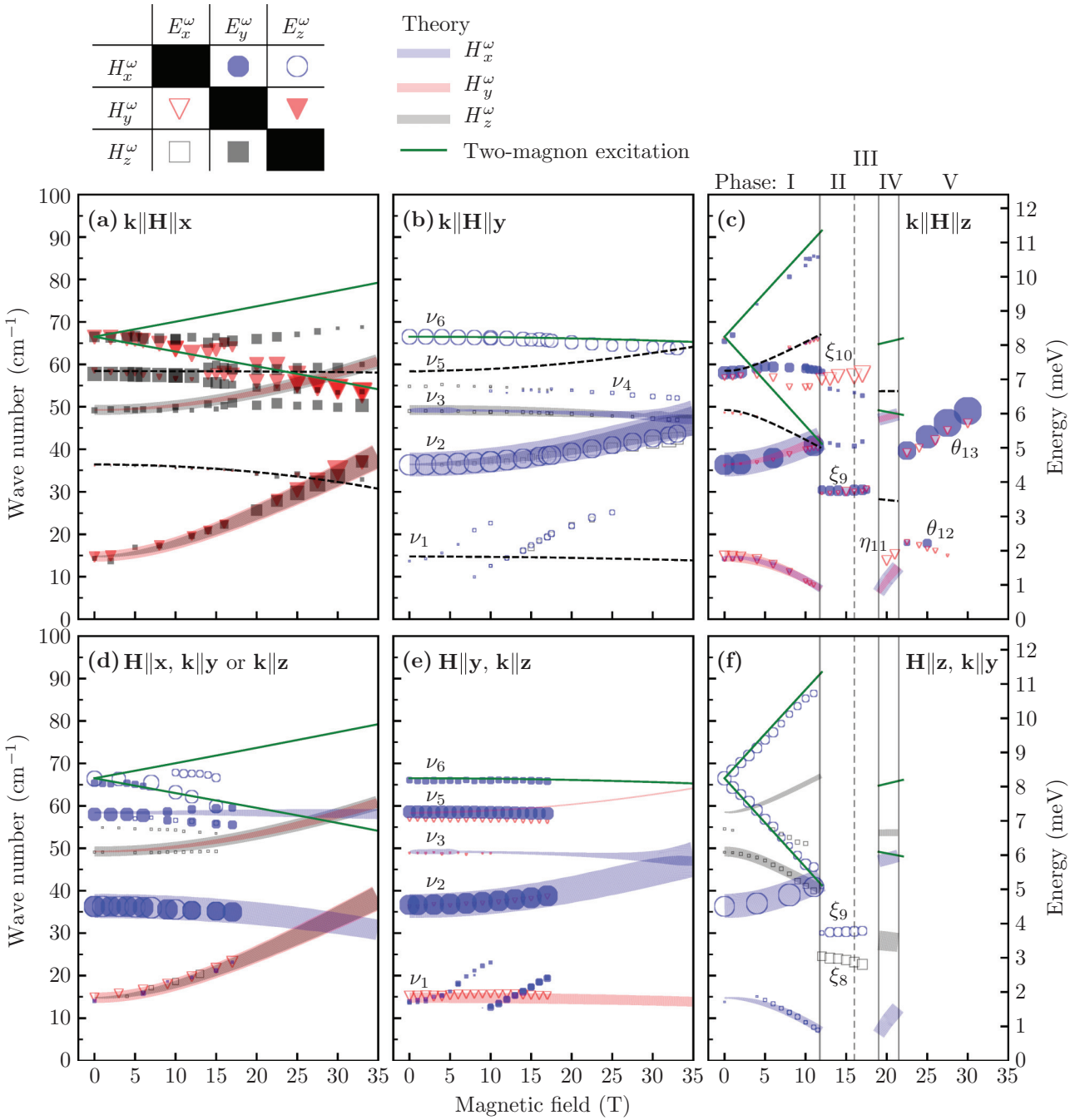

FIG. 4. Magnetic field dependence of the magnon resonance frequencies and absorption line areas at $T = 3.5$ K. Panels (a)–(c) correspond to measurements in the Faraday ($\mathbf{k} \parallel \mathbf{H}$), while panels (d)–(f) correspond to experiments in the Voigt ($\mathbf{k} \perp \mathbf{H}$) configuration. The direction of magnetic field is (a), (d) $\mathbf{H} \parallel \mathbf{x}$, (b), (e) $\mathbf{H} \parallel \mathbf{y}$, and (c), (f) $\mathbf{H} \parallel \mathbf{z}$. Symbols are the fit results of experimentally measured resonances and correspond to six combinations of $\{E_i^\omega, H_j^\omega\}$ as indicated on top of the figure. The symbol area is proportional to the experimental absorption line area. The solid lines are the results of the model calculations based on Eqs. (1)–(7). The width of the line is proportional to the square root of the line area calculated in the magnetic dipole approximation. The color of the symbol and the line is determined by the magnetic component of light: H_x^ω, blue; H_y^ω, red; and H_z^ω, black. The line positions of modes with vanishing theoretical intensity in all measured configurations of panels (a)–(c) are shown by black dashed lines. The green solid line is the two-magnon excitation ν_6. The phase boundaries determined from the magnetic field dependence of the THz spectra are shown by vertical solid lines in (c) and (f); the phase boundary between II and III, vertical dashed line, is from Refs. [42,44].

ν_1, ν_2, ν_3, and ν_5. The magnetic field dependence and the selection rules of the magnetic-dipole active magnons ν_1, ν_2, and ν_3 are reproduced well by the mean-field model, Fig. 4. However, only the energy of the magnon ν_5 is reproduced by the model and not the intensity as this excitation is found to be an electromagnon in the experiment.

The resonances ν_4, ν_6, and the band ν_7 cannot be described within the four-sublattice mean-field model. The weak ν_4

mode is a ME spin excitation, $\{E_x^\omega, H_z^\omega\}$ active, which might be related to a spin-stretching excitation allowed for $S > 1/2$ [52]. The ν_6 mode is a ME two-magnon excitation and ν_7 is an E_x^ω-active two-magnon excitation band, as will be discussed below. The excitations ξ_8, ξ_9, ξ_{10}, and θ_{12}, θ_{13} are only present in the incommensurate phases II, III, and in phase V with more than four spins per magnetic unit cell and thus cannot be explained by the present four-sublattice model. The field dependence and the selection rules of η_{11}, the only mode found experimentally in the four-sublattice commensurate phase IV, are described by the model, Figs. 4(c) and 4(f).

There are two resonances in the vicinity of the ν_1 mode as indicated by blue symbols in Figs. 4(b) and 4(e). These two modes have a well-defined selection rule, H_x^ω. Because they are at low frequency but not described by the mean-field model we assign them to impurity modes.

The exchange parameters obtained by fitting the mean-field model to THz spectra are presented in Table I. Our model also reproduces the magnetization for commensurate phases I and IV, Fig. 2. The canting angle of spins given by the parameters of the current work, Table I and Eq. (2), is $\pm\theta = 8.1^\circ$ in zero field, in good agreement with the value determined by elastic neutron scattering, $(7.8 \pm 2.6)^\circ$, as reported in Refs. [36,39].

V. DISCUSSION

A. One-magnon excitations

The four sublattice mean-field model describes four magnons ν_1, ν_2, ν_3, and ν_5, among which ν_1 and ν_2 can be identified as Γ-point magnon modes observed in the INS spectra [37], whereas the ν_5 resonance has also been detected by the Raman spectroscopy [51].

The zero-field frequencies of ν_1 and ν_2 are related to the single-ion anisotropies Λ_x and Λ_y, respectively. Furthermore, the selection rules for the ν_1 and ν_2 suggest that they are anisotropy-gapped magnons, since in both cases the magnetic dipole moment oscillates perpendicular to the corresponding anisotropy axis, along y for the ν_1 mode and along x for ν_2 in zero field. Moreover, the mean-field model reproduces the rotation of the magnetic dipole moment of ν_1 (ν_2) towards the z axis in increasing magnetic field $\mathbf{H} \parallel \mathbf{y}$ ($\mathbf{H} \parallel \mathbf{x}$). The reappearance of ν_1 in phase IV, marked as η_{11}, is also predicted by the model.

The frequencies of ν_3 and ν_5 depend strongly on the weak J_{xy} and J_{xz} exchange interactions connecting the two AF systems, $\{\mathbf{S}_1, \mathbf{S}_4\}$ and $\{\mathbf{S}_2, \mathbf{S}_3\}$. While the FM J_{xz} only shifts the average frequency of ν_3 and ν_5, the AF J_{xy} affects the difference frequency. The zero-field selection rules of these excitations—magnetic dipole moment along z for ν_3 and the absence of magnetic-dipole activity of ν_5—are reproduced by the model.

Our model does not describe the incommensurate phases II, III, and V. However, it reproduces the frequency of the lowest η_{11} mode in the commensurate phase IV, Fig. 4(c).

B. Two-magnon excitations

Two-magnon excitations appear in the absorption spectra when one absorbed photon creates two magnons with the total $\mathbf{k}$ vector equal to zero [53]. The two-magnon absorption is the strongest where the density of magnon states is the highest, usually at the Brillouin-zone boundary. Since the product of the two spin operators has the same time-reversal parity as the electric dipole moment, the two-magnon excitation by the electric field is allowed; this mechanism usually dominates over the magnetic-field-induced two-magnon excitation [53].

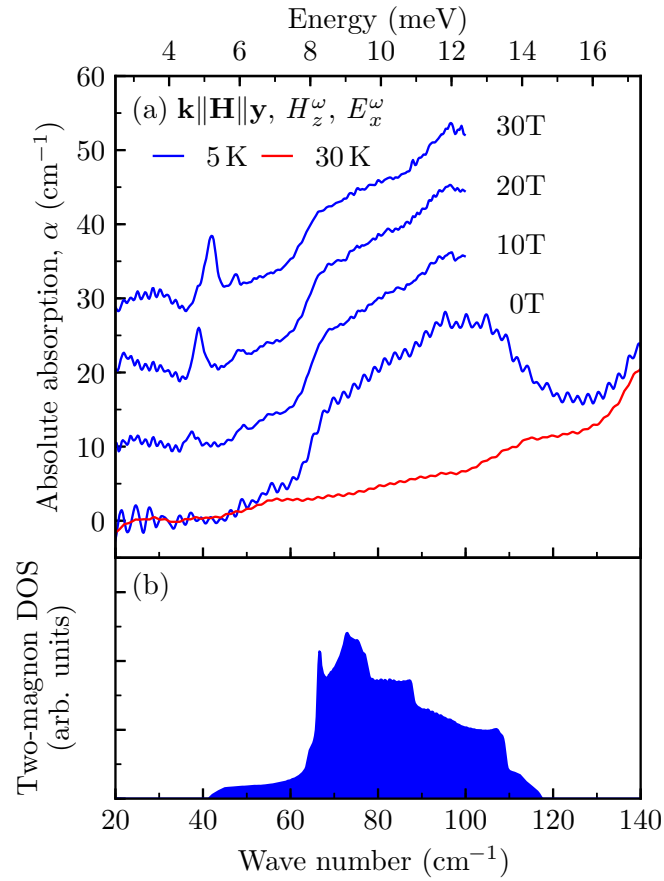

FIG. 5. (a) Two-magnon excitation band ν_7 in $LiNiPO_4$ as observed in the experiment (blue spectra). (b) Calculated two-magnon density of states. The two-magnon absorption is absent in the paramagnetic state, red line in panel (a), measured in 0 T at 30 K. All spectra are first shifted to zero absorption at 20 cm^{-1} and then a constant shift proportional to the field is added. The spectra in magnetic field were measured up to 100 cm^{-1}.

The broad absorption band between 60 and 115 cm^{-1}, shown in Fig. 5(a), appears below T_N and is E_x^ω active. A similar excitation band observed by Raman scattering was attributed to spin excitations [51]. In another olivine-type crystal $LiMnPO_4$, a broad band in the Raman spectrum was assigned to a two-magnon excitation with the line shape reproduced using the magnon density of states (DOS) [54].

We calculated the magnon DOS numerically on a finite-size sample of $4 \times 4 \times 4$ unit cells with 256 spins using the model represented by Eq. (1) but extended by the J_y and J_z couplings shown in Fig. 1. The two-magnon DOS was obtained by doubling the energy scale of the single-magnon DOS and is shown in Fig. 5(b). Since the observed broad absorption band emerges in the energy range of the high magnon DOS we assign this absorption band to a two-magnon excitation.

There is another dominantly electric-dipole active spin resonance ν_6 at 66.5 cm^{-1} not reproduced by our mean-field model. Since the frequency of the electric-dipole active ν_6 mode is at the maximum of the two-magnon DOS and in a magnetic field, $\mathbf{H} \parallel \mathbf{z}$, splits into a lower and an upper resonances with effective g factors $g_- = 4.24 \pm 0.07$ and $g_+ = 4.00 \pm 0.04$, i.e., two times larger than that expected for one spin-flip excitation, we interpret the ν_6 resonance as a two-magnon excitation. The singular behavior in the DOS coinciding with the ν_6 resonance peak corresponds to the flat magnon dispersion along the *R*–*T* line in the Brillouin zone. This mode is weakly magnetic-dipole active as well and is therefore a ME resonance.

The magnetic field dependence of the two-magnon excitation ν_6 was modeled by calculating the field dependence of the magnon DOS. The result is shown in Fig. 4. The splitting of the resonance in magnetic field is observed only for $\mathbf{H} \parallel \mathbf{z}$ and is reproduced by the model calculation. In the calculation J_y was set to 0.65 meV to reproduce the instability of phase I at 12 T, while $J_z = 0.16$ meV was used to reproduce the zero-field frequency of ν_6. The magnitude of J_y and J_z is similar to the ones in INS studies [36–38] but J_z has the opposite sign. In high-symmetry cases the electric-dipole selection rules of two-magnon excitations can be reproduced by group-theoretical analysis [55], but the low magnetic symmetry of $LiNiPO_4$ hinders such an analysis. Nevertheless, it is expected that the $\Delta S = 0$ two-magnon continuum ν_7 has different selection rules than the $\Delta S = 2$ two-magnon excitation ν_6 due to their different symmetry.

VI. CONCLUSIONS

We measured the magnetic field dependence of THz absorption spectra in various magnetically ordered phases of $LiNiPO_4$. We have revealed a variety of spin resonance modes: three magnons, an electromagnon, an electric-dipole active two-magnon excitation band, and a magnetoelectric two-magnon excitation. The abrupt changes in the magnon absorption spectra coincide with the magnetic phase boundaries in $LiNiPO_4$. The magnetic dipole selection rules for magnon absorption and the magnetic field dependence of magnon frequencies in the commensurate magnetic phases are described with a mean-field spin model. With this model the additional information obtained from the magnetic field dependence of mode frequencies allowed us to refine the values of exchange couplings, single-ion anisotropies, and Dzyaloshinskii-Moriya interaction. The significant differences found in magnetic interaction parameters compared to former studies are the opposite sign of J_z exchange coupling, the smaller values of the J_{xy} exchange coupling and the Λ_x and Λ_y anisotropies. The mean-field model did not explain the observed magnetoelectric excitation ν_4 and the spin excitations in the incommensurate phases. In the future, more about the magnetoelectric nature of $LiNiPO_4$ spin excitations can be learned from nonreciprocal directional dichroism studies as in $LiCoPO_4$ [24].

ACKNOWLEDGMENTS

The authors are indebted to L. Mihály and K. Penc for valuable discussions. This project was supported by institutional research funding IUT23-3 of the Estonian Ministry of Education and Research, by European Regional Development Fund Project No. TK134, by the bilateral program of the Estonian and Hungarian Academies of Sciences under the Contract No. NKM-47/2018, by the Hungarian NKFIH Grant No. ANN 122879, by the BME Nanotechnology and Materials Science FIKP grant of EMMI (BME FIKP-NAT), and by the Deutsche Forschungsgemeinschaft (DFG) via the Transregional Research Collaboration TRR 80: From Electronic Correlations to Functionality (Augsburg-Munich-Stuttgart). D.S. acknowledges the FWF Austrian Science Fund I Grant No. 2816-N27 and V.K. was supported by the RIKEN Incentive Research Project. High magnetic field experiments were supported by HFML-RU/NWO-I, member of the European Magnetic Field Laboratory (EMFL).

L.P., V.K., and D. S. contributed equally to this work.

[1] T. Kimura, T. Goto, H. Shintani, K. Ishizaka, T. Arima, and Y. Y. Tokura, Nature (London) **426**, 55 (2003).
[2] M. Fiebig, J. Phys. D: Appl. Phys. **38**, R123 (2005).
[3] N. A. Spaldin and M. Fiebig, Science **309**, 391 (2005).
[4] W. Eerenstein, N. D. Mathur, and J. F. Scott, Nature (London) **442**, 759 (2006).
[5] S.-W. Cheong and M. Mostovoy, Nat. Mater. **6**, 13 (2007).
[6] M. Fiebig and N. A. Spaldin, Eur. Phys. J. B **71**, 293 (2009).
[7] S. Dong, J.-M. Liu, S.-W. Cheong, and Z. Ren, Adv. Phys. **64**, 519 (2015).
[8] M. Fiebig, T. Lottermoser, D. Meier, and M. Trassin, Nat. Rev. Mater. **1**, 16046 (2016).
[9] G. L. J. A. Rikken and E. Raupach, Nature (London) **390**, 493 (1997).
[10] G. L. J. A. Rikken, C. Strohm, and P. Wyder, Phys. Rev. Lett. **89**, 133005 (2002).
[11] L. D. Barron, *Molecular Light Scattering and Optical Activity*, 2nd ed. (Cambridge University Press, Cambridge, UK, 2004).
[12] T. Arima, J. Phys.: Condens. Matter **20**, 434211 (2008).
[13] D. Szaller, S. Bordács, V. Kocsis, T. Rõõm, U. Nagel, and I. Kézsmárki, Phys. Rev. B **89**, 184419 (2014).
[14] I. Kézsmárki, N. Kida, H. Murakawa, S. Bordács, Y. Onose, and Y. Tokura, Phys. Rev. Lett. **106**, 057403 (2011).
[15] S. Bordács, I. Kézsmárki, D. Szaller, L. Demkó, N. Kida, H. Murakawa, Y. Onose, R. Shimano, T. Rõõm, U. Nagel *et al.*, Nat. Phys. **8**, 734 (2012).
[16] Y. Takahashi, R. Shimano, Y. Kaneko, H. Murakawa, and Y. Tokura, Nat. Phys. **8**, 121 (2012).
[17] I. Kézsmárki, D. Szaller, S. Bordács, V. Kocsis, Y. Tokunaga, Y. Taguchi, H. Murakawa, Y. Tokura, H. Engelkamp, T. Rõõm *et al.*, Nat. Commun. **5**, 3203 (2014).
[18] I. Kézsmárki, U. Nagel, S. Bordács, R. S. Fishman, J. H. Lee, H. T. Yi, S.-W. Cheong, and T. Rõõm, Phys. Rev. Lett. **115**, 127203 (2015).
[19] A. M. Kuzmenko, V. Dziom, A. Shuvaev, A. Pimenov, M. Schiebl, A. A. Mukhin, V. Y. Ivanov, I. A. Gudim, L. N.

Bezmaternykh, and A. Pimenov, Phys. Rev. B **92**, 184409 (2015).
[20] S. Bordács, V. Kocsis, Y. Tokunaga, U. Nagel, T. Rõõm, Y. Takahashi, Y. Taguchi, and Y. Tokura, Phys. Rev. B **92**, 214441 (2015).
[21] Y. Okamura, F. Kagawa, S. Seki, M. Kubota, M. Kawasaki, and Y. Tokura, Phys. Rev. Lett. **114**, 197202 (2015).
[22] Y. Nii, R. Sasaki, Y. Iguchi, and Y. Onose, J. Phys. Soc. Jpn. **86**, 024707 (2017).
[23] S. Yu, B. Gao, J. W. Kim, S.-W. Cheong, M. K. L. Man, J. Madéo, K. M. Dani, and D. Talbayev, Phys. Rev. Lett. **120**, 037601 (2018).
[24] V. Kocsis, K. Penc, T. Rõõm, U. Nagel, J. Vít, J. Romhányi, Y. Tokunaga, Y. Taguchi, Y. Tokura, I. Kézsmárki *et al.*, Phys. Rev. Lett. **121**, 057601 (2018).
[25] J. Viirok, U. Nagel, T. Rõõm, D. G. Farkas, P. Balla, D. Szaller, V. Kocsis, Y. Tokunaga, Y. Taguchi, Y. Tokura *et al.*, Phys. Rev. B **99**, 014410 (2019).
[26] Y. Okamura, S. Seki, S. Bordács, A. Butykai, V. Tsurkan, I. Kézsmárki, and Y. Tokura, Phys. Rev. Lett. **122**, 057202 (2019).
[27] A. Pimenov, A. A. Mukhin, V. Y. Ivanov, V. D. Travkin, A. M. Balbashov, and A. Loidl, Nat. Phys. **2**, 97 (2006).
[28] M. Mercier and J. Gareyte, Solid State Commun. **5**, 139 (1967).
[29] M. Mercier, J. Gareyte, and E. F. Bertaut, C. R. Acad. Sci. Paris **264**, 979 (1967).
[30] M. Mercier and P. Bauer, C. R. Acad. Sci. Paris **267**, 465 (1968).
[31] M. Mercier, E. F. Bertaut, G. Quézel, and P. Bauer, Solid State Commun. **7**, 149 (1969).
[32] J.-P. Rivera, Ferroelectrics **161**, 147 (1994).
[33] I. Kornev, M. Bichurin, J.-P. Rivera, S. Gentil, H. Schmid, A. G. M. Jansen, and P. Wyder, Phys. Rev. B **62**, 12247 (2000).
[34] R. Toft-Petersen, M. Reehuis, T. B. S. Jensen, N. H. Andersen, J. Li, M. D. Le, M. Laver, C. Niedermayer, B. Klemke, K. Lefmann *et al.*, Phys. Rev. B **92**, 024404 (2015).
[35] V. M. Khrustalyov, V. N. Savytsky, and M. F. Kharchenko, Low Temp. Phys. **43**, 1332 (2017).
[36] R. Toft-Petersen, J. Jensen, T. B. S. Jensen, N. H. Andersen, N. B. Christensen, C. Niedermayer, M. Kenzelmann, M. Skoulatos, M. D. Le, K. Lefmann, S. R. Hansen, J. Li, J. L. Zaretsky, and D. Vaknin, Phys. Rev. B **84**, 054408 (2011).
[37] T. B. S. Jensen, N. B. Christensen, M. Kenzelmann, H. M. Rønnow, C. Niedermayer, N. H. Andersen, K. Lefmann, M. Jiménez-Ruiz, F. Demmel, J. Li *et al.*, Phys. Rev. B **79**, 092413 (2009).
[38] J. Li, T. B. S. Jensen, N. H. Andersen, J. L. Zarestky, R. W. McCallum, J.-H. Chung, J. W. Lynn, and D. Vaknin, Phys. Rev. B **79**, 174435 (2009).
[39] T. B. S. Jensen, N. B. Christensen, M. Kenzelmann, H. M. Rønnow, C. Niedermayer, N. H. Andersen, K. Lefmann, J. Schefer, M. Zimmermann, J. Li *et al.*, Phys. Rev. B **79**, 092412 (2009).
[40] Y. N. Kharchenko, N. F. Kharcheno, M. Baran, and R. Szymczak, Low Temp. Phys. **29**, 579 (2003).
[41] D. Vaknin, J. L. Zarestky, J.-P. Rivera, and H. Schmid, Phys. Rev. Lett. **92**, 207201 (2004).
[42] V. Khrustalyov, V. Savitsky, and N. Kharchenko, Czech. J. Phys. **54**, 27 (2004).
[43] V. M. Khrustalyov, V. M. Savytsky, and M. F. Kharchenko, Low Temp. Phys. **42**, 1126 (2016).
[44] R. Toft-Petersen, E. Fogh, T. Kihara, J. Jensen, K. Fritsch, J. Lee, G. E. Granroth, M. B. Stone, D. Vaknin, H. Nojiri *et al.*, Phys. Rev. B **95**, 064421 (2017).
[45] P. J. Baker, I. Franke, F. L. Pratt, T. Lancaster, D. Prabhakaran, W. Hayes, and S. J. Blundell, Phys. Rev. B **84**, 174403 (2011).
[46] O. García-Moreno, M. Alvarez-Vega, J. García-Jaca, J. M. Gallardo-Amores, M. L. Sanjuán, and U. Amador, Chem. Mater. **13**, 1570 (2001).
[47] R. Santoro, D. Segal, and R. Newnham, J. Phys. Chem. Solids **27**, 1192 (1966).
[48] D. Vaknin, J. L. Zarestky, J. E. Ostenson, B. C. Chakoumakos, A. Goñi, P. J. Pagliuso, T. Rojo, and G. E. Barberis, Phys. Rev. B **60**, 1100 (1999).
[49] R. M. White, *Quantum Theory of Magnetism* (Springer-Verlag, Berlin, Heidelberg, 2007).
[50] T. L. Gilbert, IEEE Trans. Magn. **40**, 3443 (2004).
[51] V. I. Fomin, V. P. Gnezdilov, V. S. Kurnosov, A. V. Peschanskii, A. V. Yeremenko, H. Schmid, J.-P. Rivera, and S. Gentil, Low Temp. Phys. **28**, 203 (2002).
[52] K. Penc, J. Romhányi, T. Rõõm, U. Nagel, A. Antal, T. Fehér, A. Jánossy, H. Engelkamp, H. Murakawa, Y. Tokura *et al.*, Phys. Rev. Lett. **108**, 257203 (2012).
[53] P. L. Richards, J. Appl. Phys. **38**, 1500 (1967).
[54] C. C. Filho, P. Gomes, A. García-Flores, G. Barberis, and E. Granado, J. Magn. Magn. Mater. **377**, 430 (2015).
[55] R. Loudon, Adv. Phys. **17**, 243 (1968).